Agr. Nat. Resour. 57 (2023) 321–330

AGRICULTURE AND NATURAL RESOURCES

Journal homepage: http://anres.kasetsart.org

Research article

Application of pulse width modulation technique in air humidity control system

Aphisik Pakdeekaew[a,†], Krawee Treeamnuk[a,*], Tawarat Treeamnuk[b], Nuttapong Wongbubpa[c,†]

[a] *School of Mechanical Engineering, Institute of Engineering, Suranaree University of Technology, Nakhon Ratchasima 30000, Thailand*

[b] *School of Agricultural Engineering, Institute of Engineering, Suranaree University of Technology, Nakhon Ratchasima 30000, Thailand*

[c] *School of Mechatronics Engineering, Faculty of Engineering and Technology, Rajamangala University of Technology Isan, Nakhon Ratchasima 30000, Thailand*

Article Info

Article history:
Received 28 November 2022
Revised 17 March 2023
Accepted 25 March 2023
Available online 30 April 2023

Keywords:
Adiabatic mixing process,
Air humidity ratio,
Proportional-integral-derivative (PID) control,
Pulse width modulation,
Ziegler-Nichols' 2nd method

Abstract

Importance of the work: A method was presented for controlling the humidity ratio of the mixture of emitted air from a dryer with fresh air so that it can be applied to reduce energy consumption in the future.

Objectives: To develop a control system with a pulse width modulation (PWM) technique for air humidity ratio control in a laboratory-scale paddy drying system.

Materials & Methods: An on-off air control valve with PWM was controlled using two methods: 1) theoretical calculation; and 2) the second of Ziegler-Nichol's methods consisting of Proportional-integral (PI)-, Proportional-integral-derivative (PID)- and PID-no overshoot controls, respectively.

Results: A closed-loop control system based on Ziegler-Nichols' second method achieved the fastest steady-state response, especially with a PID controller. The performance of Ziegler-Nichols' second method was closer to the reference values at a steady state than the theoretical calculation method.

Main finding: All the proposed methods produced low error in steady-state responses with averages less than 3.691%. All methods were suitable for various applications, with sufficient potential for application in controlling the humidity ratio of air in the drying process of agricultural products.

† Equal contribution.

* Corresponding author.
E-mail address: krawee@sut.ac.th (K. Treeamnuk)

https://doi.org/10.34044/j.anres.2023.57.2.12

Introduction

Agricultural products are important to human life, especially grain foods such as rice, wheat, corn and beans, because of their high nutritional benefits and capacity to be processed into a variety of foods (IMPOFF, 2022; International Rice Research Institute, 2022a). Drying is an important process after harvesting as it can prevent problems of high moisture content in the crop which results in the growth of fungi or microorganisms and leads to the deterioration of the quality of the produce in storage (International Rice Research Institute, 2022b; Müller et al., 2022). Various types of mechanical dryers have been developed using different techniques depending on the purpose of drying and its cost-effectiveness for the product (Aghbashlo et al., 2013; Indiarto et al., 2021). Grain can be dried with a variety of hot-air dryers, such as drying paddy using the Lousiana State University so-called LSU dryer (Jittanit et al., 2010; Vengsungnle et al., 2018), drying paddy using a rotary dryer (Firouzi et al., 2017) and drying corn using a fluidized bed dryer (Khanali et al., 2018). A review of past research showed that hot-air dryers consume very high energy. For example, the LSU dryer which is very popular in the grain industry, has an energy consumption of 3.874–6.25 MJ/kg-water (Jittanit et al., 2010; Mondal et al., 2019), while the energy consumption ranges for the must-flow paddy dryer and the rotary paddy dryer were 1.94–3.89 MJ/kg-water (Mustafa et al., 2014; Tuaynak et al., 2014) and 2.64–9.2 MJ/kg-water (Firouzi et al., 2017; Havlík et al., 2020), respectively. Exhaust air recirculation can be used to reduce energy consumption in a hot-air dryer. Recently, Sila et al. (2022) indicate that a high volumetric proportion of air circulation leads to the reduction of energy consumption in air heating systems. This effect was supported by Darvishi et al. (2018), who investigated the effects of osmotic pretreatment and air recirculation on energy and exergy analyses of a fluidized bed drying sliced mushrooms under different drying conditions. It was also similar to the research of Afzali et al. (2019), which stated that the percentage of air convection was one factor affecting the exergetic performance of a conveyor infrared hot-air dryer for mushroom slices. However, grains are natural biomaterials, which are very sensitive to rapid changes in air temperature and air humidity, especially in dryers. This may directly affect the quality of the product (Chayjan et al., 2019; Müller et al., 2022). Therefore, it is necessary to precisely control the recirculating air to obtain the required humidity of air mixture before entering the drying process. Pulse width modulation (PWM) is an important control technique that can be applied to a wide range of control systems. For example, Fernando et al. (2021) used the PWM technique to control the voltage supplied to the motor of a heat pump dryer to manipulate air circuit parameters. In addition, PWM has been applied to drive a pneumatic muscle actuator system using on/off solenoid valves (Jouppila et al., 2014).

The current research investigated applying the PWM technique to control the operation of a solenoid valve to achieve the desired humidity of the air mixture between exhaust recirculating air and the ambient air. It was hypothesized that precisely controlling the air circulation system would contribute to improving the energy efficiency of the dryer and improving the quality of the product after drying.

Materials and Methods

This research developed a method for controlling the humidity ratio of air based on two experiments: 1) air humidity ratio control based on the theoretical calculation method, and 2) air humidity ratio control according to the second method of Ziegler-Nichols.

Equipment

A laboratory-scale, hot-air-producing system was developed to represent an actual agricultural dryer (Fig. 1A). The system was used to evaluate the method of controlling the humidity ratio of the air mixture between the ambient air inlet (Fig. 1B, No. 1) and the humid air after receiving moisture from the spray chamber, which was recirculated in different proportions (Fig. 1B, No. 2). The components of the system are shown in Fig. 1B.

From Fig. 1B, this system used a direct current (DC) blower (24 V 5.5 A at 3,700 revolutions per minute) to recirculate the air. Ambient air flowed into the system through the Venturi flow meter at No. 1 (Arduino pressure sensor, HX710B modules and DHT22 (AM2302 modules, with relative humidity (RH) accurate to ±2% (maximum ±5% RH); temperature < ±0.5 °C; operating range for humidity 0–100%, for temperature -40 °C to approximately 80 °C (Components 101, 2018); and the air was regulated to

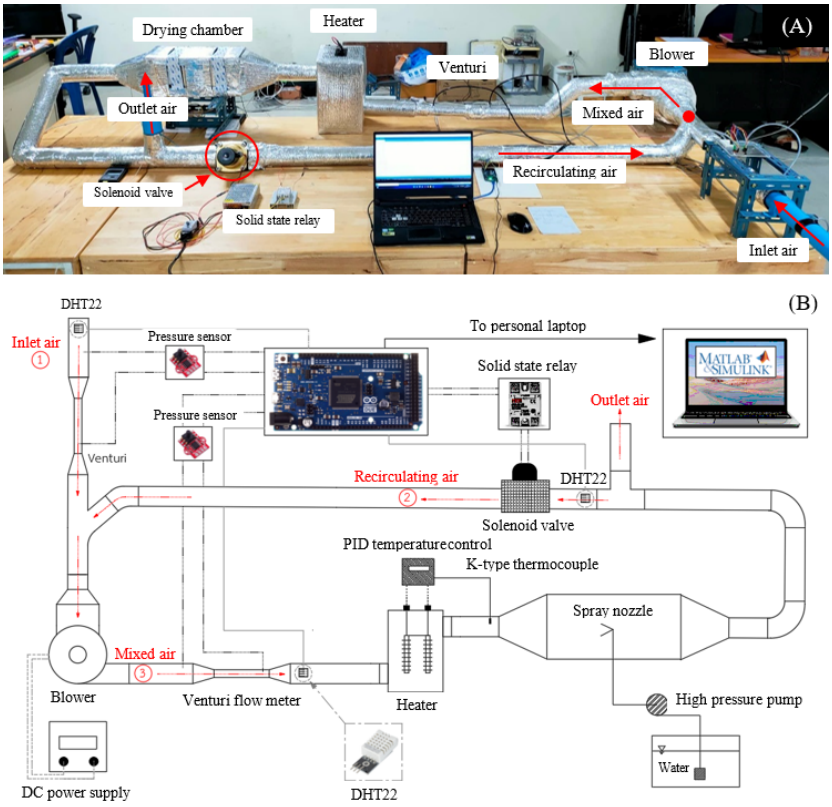

Fig. 1 (A) Laboratory-scale drying system for experimentation; (B) diagram of laboratory-scale drying system

a constant velocity of 6 m/s at No. 3 by a voltage regulator DC power supply (ATTEN model APR3010H) throughout the test (constant volumetric flow of 0.015 m^3/s). The air was heated with a heater according to the heating process. It worked separately from the main control system under a proportional-integral-derivative (PID) temperature controller (RKG model REX-C100FK02) to control the air at a constant temperature of 80 °C before entering the drying chamber. Water spray was used to represent the remaining moisture in the material in the actual drying process in the drying chamber. This method maintained a constant air humidification rate throughout the experiment instead of the actual drying material in the dryer. A nozzle inside the chamber sprayed water using a high-pressure pump (SEAFLO model SFDP1-013-100-22, 12 V, 5 A, pressure 690 kPa) to create pressure for the spraying system. When the hot air met the water mist, a heat and mass transfer process occurred. Consequently, the air temperature decreased and the RH increased (Pakdeekaew, 2021). The air properties at each measuring point were monitored using a DHT22 sensor (ASAIR model AM2302) and an Arduino DUE board was used as a microcontroller to control the system.

Pulse width modulation for airflow control using on-off solenoid valve

PWM (Dunn, 2005) is a technique to generate a digital signal that is a pulse signal with a constant period. Signals have two types of status, either 1 or HIGH or 0 or LOW, as shown in Fig. 2.

The duty cycle (Equation 1) was calculated by comparing the percentage between HIGH states in each period (Barrett and Pack, 2005):

$$Duty\ cycle = \left(\frac{Time\ HIGH}{Period}\right) \times 100\% \quad (1)$$

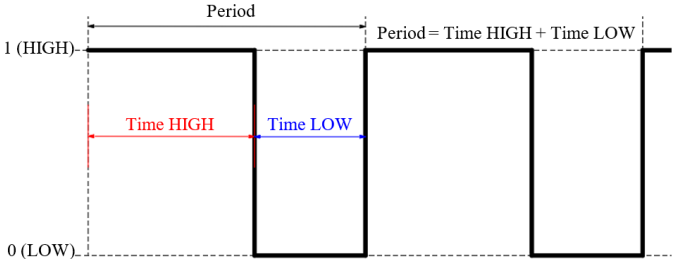

Fig. 2 Characteristics of a pulse width modulation signal

where duty cycle is the percentage of 'high' status time (in seconds) in each period (in seconds). The duty cycle is applied to operate an on/off solenoid valve (Fig. 1B) to adjust the proportion of exhaust air recirculation mixing with ambient air. The valve activation periods were proportional to the volume flow rate of the recirculated air.

The solenoid valve on-off period was defined by the percentage of duty cycle as the input signal having percentage values of 0, 20, 40, 60, 80, and 100 of the 0.2 s periods (Fig. 3). The response of the volumetric flow rate of recirculating air (Fig. 1B) was measured using the Venturi flow meter at No. 3. The coefficient of determination (R^2) and correlation coefficient (r) were used to evaluate the relation between the volume flow rate of air (in cubic meters per second) and the duty cycle (as a percentage).

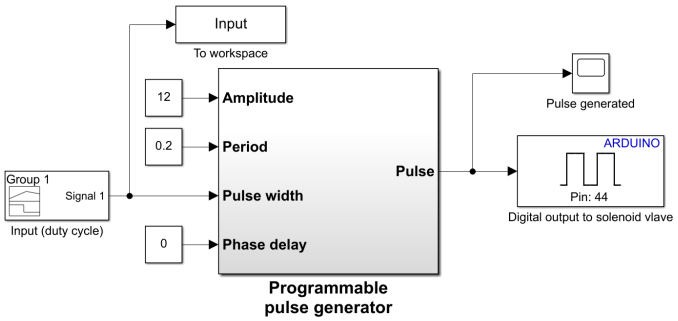

Fig. 3 Block diagram for operating solenoid valve

Air humidity ratio control using theoretical calculation method

Adiabatic mixing process of air streams

Cengel and Boles (2011) indicated that an adiabatic process is a thermodynamic process in which no heat is transferred in or out of the system ($\Delta Q = 0$). Air mixing is based on this process. The humid air mixing process is generally described in Fig. 4.

Mass balance and energy balance for the adiabatic mixing process of air streams from Fig. 3 are shown as Equations 2–4 (Cengel and Boles, 2011). The volumetric flow rate of recirculating air (Fig. 1B at No. 3) can be estimated by applying the mass balance of air humidity according to Equation 3 and dividing by the air density during the experiment:

Mass balance of dry air: $\dot{m}_{a1} + \dot{m}_{a2} = \dot{m}_{a3}$ (2)

Mass balance of air humidity: $\dot{m}_{a1}\omega_1 + \dot{m}_{a2}\omega_2 = \dot{m}_{a3}\omega_3$ (3)

Energy balance: $\dot{m}_{a1}h_1 + \dot{m}_{a2}h_2 = \dot{m}_{a3}h_3$ (4)

where $\dot{m}_{ai}$ is the mass flow rate of dry air (in kilograms per second), ω_i is air humidity ratio (in kg of water, kg_{water}, divided by kilograms of dry air, kg_{da}), h_i is the enthalpy of air (in kilojoules per kilogram of dry air) and i is the state number (i = 1, 2, 3).

Calculation of air humidity ratio

Dry bulb temperature (T_{db}) and RH data from the DHT22 sensors were obtained at each measurement point (Fig. 1B) and used to calculate the approximate value of the air humidity ratio for every position. Initially, T_{db} was converted to Kelvin (K) before calculating the saturated vapor pressure (P_{sv}) using Equation 5 (American Society of Heating, Refrigerating and Air-Conditioning Engineers, 2009), while the RH was used for calculating the vapor pressure (P_v) according to Equation 6 (American Society of Heating, Refrigerating and Air-Conditioning Engineers, 2009). The values of P_v were used to determine the humidity ratio of air according to Equation 7 (American Society of Heating, Refrigerating and Air-Conditioning Engineers, 2009). The procedure can be written with a block diagram by MATLAB Simulink as shown in Fig. 5.

$$P_{sv} = exp\left(\frac{C_1}{T_{db}} + C_2 + C_3 T_{db} + C_4 T_{db}^{\ 2} + C_5 T_{db}^{\ 3} + C_6 \ln T_{db}\right) \quad (5)$$

$$P_v = \frac{RH \times P_{sv}}{100} \quad (6)$$

$$\omega = 0.621945 \times \left(\frac{P_v}{P_{atm} - P_v}\right) \quad (7)$$

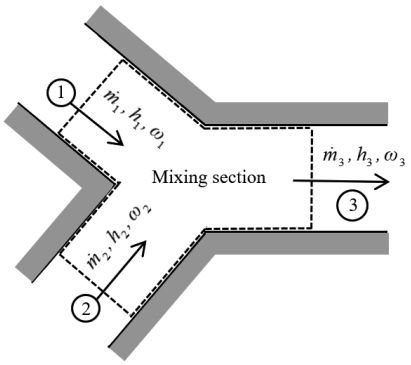

Fig. 4 Humid air mixing diagram (Cengel and Boles, 2011), where $\dot{m}_i$ is the mass flow rate of dry air (in kilograms per second), ω_i is air humidity ratio (in kg of water, kg_{water}, divided by kilograms of dry air, kg_{dryair}), h_i is the enthalpy of air (in kilojoules per kilogram of dry air) and i is the state number (i = 1, 2, 3)

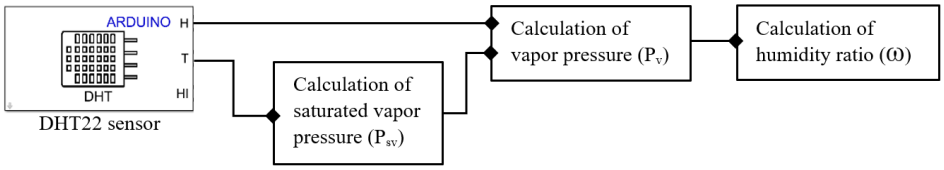

Fig. 5 Block diagram of air humidity ratio calculation

where C_1 is -5.8002206 × 10^3, C_2 is 1.3914993, C_3 is -4.8640239 × 10^{-2}, C_4 is 4.1764768 × 10^{-5}, C_5 is -1.4452093 × 10^{-8}, C_6 is 6.5459673, P_{atm} is atmospheric pressure (101,325 Pa), T_{db} is dry bulb temperature, RH is relative humidity, and P_v is the vapor pressure, ω is the air humidity ratio and P_{sv} is the saturated vapor pressure.

Theoretical calculation method controller

The theoretical Equations 2–7 were programmed into a computer to control the humidity ratio of mixed air compared to the reference value. T_{db} and RH at No. 1 and 2 (Fig. 1B) were calculated for the air humidity ratio according to Fig. 5. At the same time, the mass air flow rate measured using the Venturi flow meter and T_{db} were provided as input to the program based on Equation 3 to calculate the air flow rate at No. 2 (Fig. 1B). In addition, the relationship between the duty cycle and the recirculating air flow rate was used to configure the PWM and was used as the signal to drive the solenoid valve. A simple system operation diagram is shown in Fig. 6. The air humidity ratio after an adiabatic mixing process was compared for performance with the reference value.

Air humidity ratio control according to second method of Ziegler-Nichols

Proportional-integral-derivative control

PID control is a feedback control (Fig. 7) in which the operation can be designed and tuned without needing to know the actual model of the system (Ogata, 2010). System error values (R(s) - Y(s)) were used for calculations in the PID controller based on three variables: the proportional term, the integral term and the derivative term, as defined in Equations 8 and 9.

$$G_{PID}(s) = K_p \times (1 + \frac{1}{T_i s} + T_d s) \quad (8)$$

$$U(s) = (K_p + K_i \frac{1}{s} + K_d s) \times E(s) \quad (9)$$

where $G_{PID}(s)$ is the PID controller transfer function, K_p is the proportional gain, K_i is the integral gain, K_d is the derivative gain, T_i is the integral time, T_d is the derivative time, U(s) is the control signal and E(s) is the error signal.

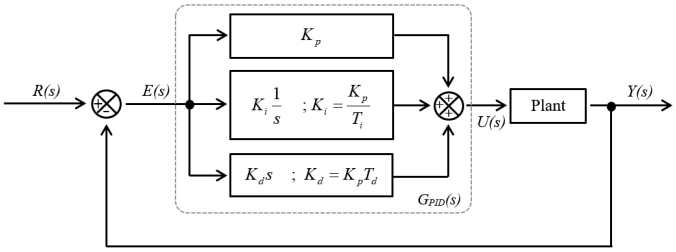

Fig. 7 Block diagram of proportional-integral-derivative control system, where R(s) is the reference input signal, E(s) is the error signal, $G_{PID}(s)$ is the PID controller transfer function, K_p is the proportional gain, K_i is the integral gain, K_d is the derivative gain, T_i is the integral time, T_d is the derivative time, U(s) is the control signal, Plant is the combination of process and actuator and Y(s) is the output signal

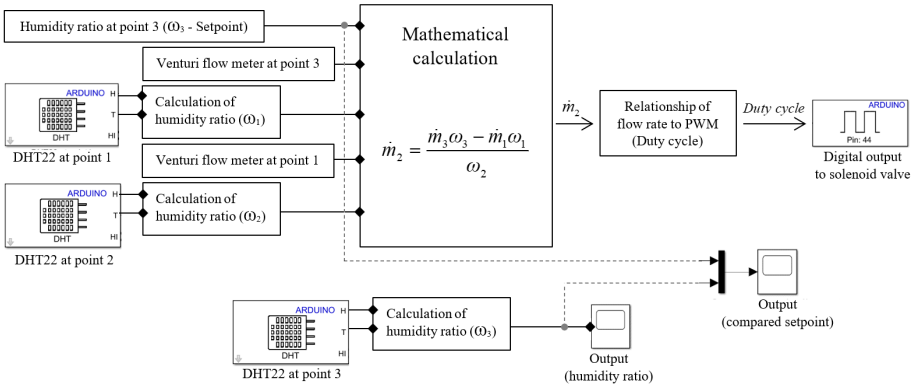

Fig. 6 Block diagram of theoretical calculation method controller, where Duty cycle is the percentage of 'high' status time (in seconds) in each period (in seconds), PWM is pulse width modulation

Ziegler-Nichols' second method was used to adjust the parameters in the PID control system. The system adjustment began by tuning only the proportional feedback control system (K_i, K_d = 0) (Ogata, 2010) until K_p equaled the critical gain (K_{cr}). During this time, the ratio of air humidity (output) was oscillating, as shown in Fig. 8, and the oscillation period (P_{cr}) and critical gain (K_{cr}) were measured and used for calculating the variables, as shown in Table 1. In this experiment, three type of controllers were studied: the unmodified PI, PID, and PID-no overshoot controls.

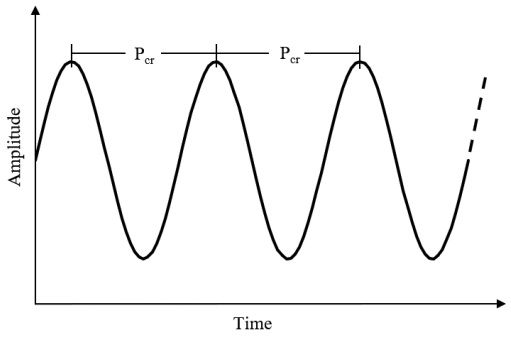

Fig. 8 Sustained oscillation with period P_{cr}

Table 1 Gain calculation from various controllers

Type of controller	K_p §	K_i ‖	K_d ¶
PI (Ogata, 2010)*	0.45 K_{cr}	0.54 P_{cr}	-
PID (Ogata, 2010)†	0.6 K_{cr}	1.2 K_{cr}/P_{cr}	0.075 K_{cr}/P_{cr}
PID-no overshoot (McCormack and Godfrey, 1998)‡	0.2 K_{cr}	0.4 K_{cr}/P_{cr}	0.066 K_{cr}/P_{cr}

* PI = Proportional-integral controller; † PID = Proportional-integral-derivative controller; ‡ PID-no overshoot = Proportional-integral-derivative no overshoot controller; § K_p = the proportional gain; ‖ K_i = the integral gain; ¶ K_d = the derivative gain

The duty cycle was input for the solenoid valve operation; the air humidity ratio at No. 3 (Fig. 1B) was the output of the system. This system used only one DHT22 sensor to measure the air properties at the output and to feed the data back to compare with the reference value.

Performance evaluation of developed air humidity ratio control system

The performance of the control system in each method was assessed based on the following variables:

1. The slope of the graph ($Slope_{int}$) was analyzed at the beginning of the response, approximately in the linear range.

2. The setting time (T_s) is the amount of time it takes for the system to start responding until its output converges to a steady state and gives ≤ 2% error compared to the setpoint.

3. The maximum overshoot (M_p) is the ratio of the overshoot value to the steady state value, calculated using Equation 10 (Ogata, 2010):

$$M_p = \left(\frac{\omega_{max} - \omega_{ss}}{\omega_{ss}} \right) \times 100\% \quad (10)$$

4. The root means error (RMSE) was used to analyze data consistency between the process response (ω_{output}) and the steady-state response (ω_{ss}), and then in turn was used to analyze the response after the setting time. It was calculated using Equation 11 (Chen and Lee, 2015):

$$RMSE = \sqrt{\frac{1}{n}\sum_{i=1}^{n}(\omega_{output} - \omega_{setpoint})^2} \quad (11)$$

where ω_{max} is the maximum humidity ratio, ω_{ss} is the humidity ratio at steady state, $\omega_{setpoint}$ is the setpoint of the humidity ratio and ω_{output} is the output of the humidity ratio, with all these parameters measured in kilograms of water per kilogram of dry air, with n being the number of data items.

Results and Discussion

Relationship between pulse width modulation signals and circulating air flow rate

The effect on the volumetric flow rate of circulating air when receiving various input signals (duty cycles) is shown in Fig. 9.

The correlation trend between variables was highly linear, as shown in Equation 12 with an R^2 value of 0.9988 (r = 0.9993):

$$y = (3 \times 10^{-5})\, x - 10^{-18} \quad (12)$$

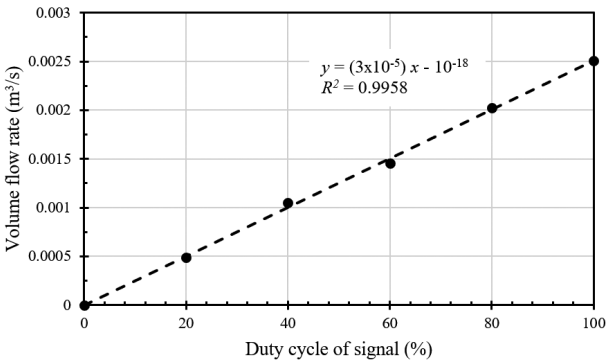

Fig. 9 Relationship between signal duty cycle and volumetric flow rate of recirculating air, where R^2 is coefficient of determination

where y is the volume flow rate of air (in cubic meters per second) and x is the duty cycle as a percentage.

These results indicated that the amount of air recirculation at No. 2 was linearly proportional to the duration of the valve (duty cycle). Based on Equation 12, the experimental results showed the percentage of recirculating air flow within the system, which can be seen in Fig. 10.

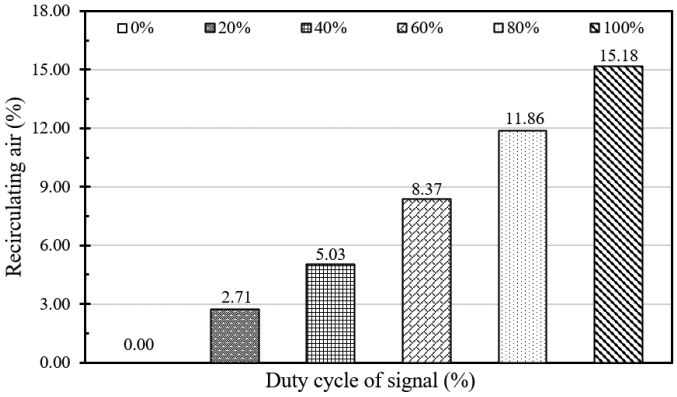

Fig. 10 Percentage of air recirculation at different inputs

The input signals (duty cycle) of 0%, 20%, 40%, 60%, 80% and 100% resulted in return air ratios of 0%, 2.71%, 5.03%, 8.37%, 11.86%, and 15.18%, respectively. The results revealed the limitations of the solenoid valves used in recirculation systems which allowed a maximum return of 15.18% air flow under these test conditions, with this restriction due to the physical characteristics of globe valves with a high pressure drop. This behavior was similar to the characteristics of manually operated globe valves in the air recirculation experiment of Sila et al. (2022). Therefore, using a low pressure drop valve is an option to increase the recirculating air and is suitable for application in an actual drying system.

Air humidity ratio control based on theoretical calculation method

The response shown in Fig. 11 shows that the mean percentage error at steady state was 3.691%. This had a slight margin of error and so this method could be applied in a wide variety of applications. The control system performance indicators are shown in Table 2. The steady-state error values were in the range 0.5–0.8% of the RMSE values. Although this method had some error gaps from the steady-state approximation, these errors can be corrected by shifting up the response with a constant corrector to compensate for the system errors and produce greater accuracy.

Air humidity ratio control based on second method of Ziegler-Nichols

The result of the PID tuning experiment using the second method of Ziegler-Nichols showed that a critical gain (K_{cr}) of 50 caused the system to oscillate, as shown in Fig. 8, with an oscillation period (P_{cr}) of 15.61 s. The gain values for each controller are shown in Table 3 and the system response from using those controls is shown in Fig. 12.

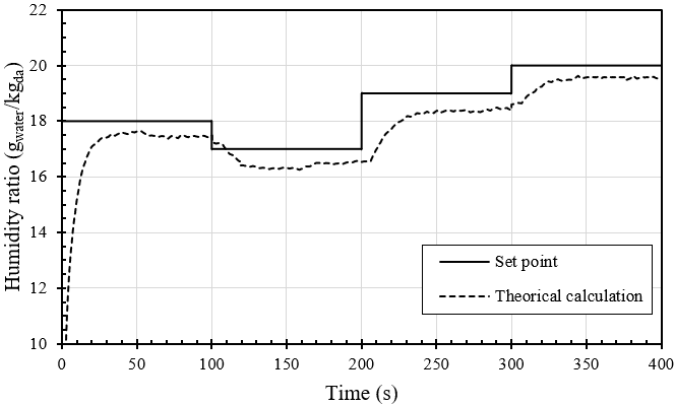

Fig. 11 Response of air humidity ratio control based on theoretical calculation method

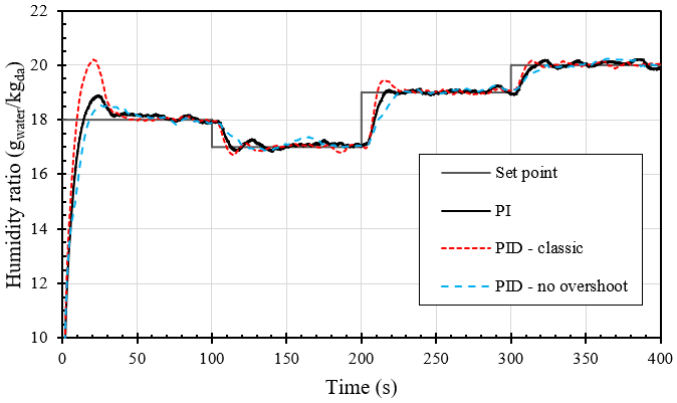

Fig. 12 Various responses of air humidity ratio control based on second method of Ziegler-Nichols

Table 2 Performance of air humidity ratio control system based on theoretical calculation method

Performance variables	Target of humidity ratio (g_{water}/kg_{da})			
	18	17	19	20
$Slope_{int}$*	0.458	-0.043	0.081	0.049
T_s (s)†	21.18	11.86	14.42	16.08
ω_{ss} (g_{water}/kg_{da})‡	17.49	16.50	18.33	19.49
RMSE§	0.533	0.589	0.778	0.489

* $Slope_{int}$ = the slope of the graph; † T_s = the setting time; ‡ ω_{ss} = the humidity ratio at steady state; § RMSE = the root means square error.

Table 3 Gain for various controllers

Type of controller	K_p[§]	K_i[‖]	K_d[¶]
PI[*]	22.5	8.4294	-
PID[†]	30	3.8436994	0.2402306
PID-no overshoot[‡]	10	1.2812299	0.2114029

* PI = Proportional-integral controller; † PID = Proportional-integral-derivative controller; ‡ PID-no overshoot = Proportional-integral-derivative no overshoot controller; § K_p = the proportional gain; ‖ K_i = the integral gain; ¶ K_d = the derivative gain

In Fig. 12, the PID controller had the highest initial response sensitivity (maximum $Slope_{int}$) compared to the other controllers across all the target humidity ratios, followed by the PI controllers, while the slowest was the PID-no overshoot controller because K_p is the main influence parameter which directly resulted in the system discrepancy in each state and resulted in the system response being extremely agile at the beginning and gradually decreasing over time. This response proportionally decreased due to the decrease in the error signal. According to the influence of K_i (the sum of the errors over all periods), when combined with K_p, it accelerated the output response reaching the reference value and substantially eliminating the remaining errors generated from K_p. Since K_i is the term that accumulated the error in the past, the system would overshoot its response, as shown in Fig. 12. The influence of K_d decreased the rate of change in response and reduced the amount of overshoot that occurred. Considering the output response, the highest M_p value was in the system with the PID controller, followed by the PI controller and the PID-no overshoot controller, respectively. According to the overview, the three control types were able to provide responses very close to the reference value in the steady-state period. The results of the evaluation of the performance of the developed control systems are shown in Table 4.

The PID controller was the fastest to converge to the equilibrium time (Ts) with a 2% error gap with the reference value except for the humidity ratio at 19 $g_{water}/g_{dry\ air}$. The PI controller provided a faster T_s response than the PID controller. For the problem of a high initial $Slope_{int}$, the PID controller took more time than the PI controller to tune itself because it had a large overshoot response at 2.11%. On the other hand, no overshoot occurred in the PI controller. In addition, the lowest RMSE values were in the range 17–19 $g_{water}/g_{dry\ air}$ because the influence of K_d in the PID controller promoted the stability of the steady-state response. The highest value of RMSE at 20 $g_{water}/g_{dry\ air}$ from the PID and PID-no overshoot controls was not much different in the steady-state range. However, the PID-no overshoot controller had a slower response time (T_s) than the other controllers in all cases and the values of M_p were lowest compared to the other controllers.

From the experiment, all the feedback control methods of air humidity ratio control were better than the theoretical calculated method. The influence of K_i in the system resulted in rapid convergence to the reference value. The RMSE (Table 4) was relatively low in the range 0.087–0.245, which was significantly lower than the theoretical calculated method. In addition, these systems used fewer sensors than the theoretical calculation method, in which two or more DHT22 sensors were used as they were needed to use the airflow measurement device. However, the actual agricultural material drying system required a long implementation time to reduce the moisture content from high-moisture agricultural materials to the storage moisture of approximately 14% wet basis for paddy (Pakdeekaew, 2021; International Rice Research Institute, 2022b). Therefore, it was not as necessary to consider the time response in the first period than the response reached in the steady-state period. All the methods had sufficient potential to be applied to air recirculation control which could contribute to energy savings when applied to various systems (Darvishi et al., 2018; Afzali et al., 2019). However, the theoretical calculation method was limited by the need for an additional flow meter in the system, which made it more complicated than the other methods that needed only DHT22 sensors.

Table 4 Performance of humidity ratio control system with various controllers

Type of controller	Performance variable	Target of humidity ratio (g_{water}/kg_{da})			
		18	17	19	20
PI[*]	$Slope_{int}$[‖]	0.780	-0.124	0.174	0.092
	T_s (s)[¶]	32.70	9.44	12.39	9.45
	M_p (%)[#]	4.22	0.71	0	0.15
	RMSE**	0.137	0.113	0.087	0.112
PID[†]	$Slope_{int}$	0.912	-0.162	0.347	0.144
	T_s (s)	31.19	7.64	18.79	7.20
	M_p (%)	11.69	1.72	2.11	0.76
	RMSE	0.093	0.105	0.088	0.245
PID – no overshoot[‡]	$Slope_{int}$	0.619	-0.040	0.102	0.045
	T_s (s)	38.82	16.39	19.30	10.99
	M_p (%)	2.91	0.59	0.38	0
	RMSE	0.143	0.159	0.113	0.278

* PI = Proportional-integral controller; † PID = Proportional-integral-derivative controller; ‡ PID-no overshoot = Proportional-integral-derivative no overshoot controller; ‖ $Slope_{int}$ = the slope of the graph; ¶ T_s = the setting time, # M_p = the maximum overshoot; ** RMSE = the root means square error

Conclusions

A technique was developed to adapt the on-off control valves with PWM for use in a feedback flow control system. The results indicated different performance of the feedback control method in the adiabatic mixing process by recirculating the humid air for the humidity ratio controlling system between the theoretical calculation method and PID control using the second method of Ziegler-Nichols. All the PID control techniques had faster response times than the theoretical calculation method and the errors in the steady-state period were also less. Controllers that combined integral and proportional controllers provided acceleration of the output response to reach the reference value. The derivative controller performed so that reduced the overshoot and converged the response aimed at the reference value. However, all the proposed methods provided low error in steady-state responses with average percentage errors of less than 3.691 and so would be suitable for use in control systems that do not need very high responsiveness. The effect of recirculating exhaust air from the dryer that retains a high temperature can reduce the power of the heater in the air heating system of the dryer because the mixing of the exhaust air and fresh air increased the temperature of the air more than from using only fresh air in the heating system. Each of these methods had sufficient potential to control the air moisture ratio in the drying process of agricultural products and could save energy in the drying system when it is further applied in a commercial scale system.

Conflict of Interest

The authors declare that there are no conflicts of interest.

Acknowledgements

This research was supported by Suranaree University of Technology.

References

Afzali, F., Darvishi, H., Behroozi-Khazaei, N. 2019. Optimizing exergetic performance of a continuous conveyor infrared-hot air dryer with air recycling system. Appl. Therm. Eng. 154: 358–367. doi.org/10.1016/j.applthermaleng.2019.03.096

Aghbashlo, M., Mobli, H., Rafiee, S., Madadlou, A. 2013. A review on exergy analysis of drying processes and systems. Renew. Sustain. Energy. Rev. 22: 1–22. doi.org/10.1016/j.rser.2013.01.015

American Society of Heating, Refrigerating and Air-Conditioning Engineers. 2009. ASHRAE handbook: Fundamentals, Atlanta, GA, USA.

Barrett, S.F., Pack, D.J. 2005. Microcontrollers fundamentals for engineers and scientists, Morgan and Claypool Publishers, San Rafael, CA, USA.

Cengel, Y.A., Boles, M.A. 2011. Thermodynamics: An Engineering Approach Seventh Edition. McGraw-Hill, New York, NY, USA.

Chayjan, R.A., Ghasemi, A., Sadeghi, M. 2019. Stress fissuring and process duration during rough rice convective drying affected by continuous and stepwise changes in air temperature. Dry. Technol. 37: 198–207. doi.org/10.1080/07373937.2018.1445637

Chen, T.-T., Lee, S.-J. 2015. A weighted LS-SVM based learning system for time series forecasting. Inf. Sci. 299: 99–116. doi.org/10.1016/j.ins.2014.12.031

Component 101. 2018. DHT22 – Temperature and humidity sensor. http://components101.com/sensors/dht22-pinout-specs-datasheet, 23 January 2023.

Darvishi, H., Azadbakht, M., Noralahi, B. 2018. Experimental performance of mushroom fluidized-bed drying: Effect of osmotic pretreatment and air recirculation. Renew. Energ. 120: 201–208. doi.org/10.1016/j.renene.2017.12.068

Dunn, W. 2005. Introduction to Instrumentation, Sensors, and Process Control. Artech House. Boston, MA, USA.

Fernando, A.J., Amaratunga, K.S.P., Dharmasena, D.A.N., Abeyrathna, R.M.R.D., Gajasinghe, I.L., Weerakoon, H.S.T., Ekanayake, E.M.A.C., Bandara, D.M.S.P. 2021. Pulse-width-modulation control of a heat pump dryer with cascade evaporators and parallel-flow condensers. Trop. Agric. Res. 33: 9–17. doi.org/10.4038/tar.v33i1.8532

Firouzi, S., Alizadeh, M.R., Haghtalab, D. 2017. Energy consumption and rice milling quality upon drying paddy with a newly–designed horizontal rotary dryer. Energy 119: 629–636. doi.org/10.1016/j.energy.2016.11.026

Havlík, J., Dlouhý, T., Sabatini, M. 2020. The effect of the filling ratio on the operating characteristics of an indirect drum dryer. Acta Polytech. 60: 49–55. doi: 10.14311/AP.2020.60.0049

IMPOFF. 2021. Importance of food in our daily life and why its necessary?. https://impoff.com/importance-of-food/, 30 July 2022.

Indiarto, R., Asyifaa, A.H., Adiningsih, F.C.A., Aulia, G.A., Achmad, S.R. 2021. Conventional and advanced food-drying technology: A current review. Int. J. Sci. Technol. Res. 10: 99–107.

International Rice Research Institute. 2022a. The Importance of Rice. Los Baños, the Philippines. http://www.knowledgebank.irri.org/ericeproduction/Importance_of_Rice.htm, 30 July 2022.

International Rice Research Institute. 2022b. Paddy drying systems. Los Baños, the Philippines. http://www.knowledgebank.irri.org/training/fact-sheets/postharvest-management/drying-fact-sheet-category/paddy-drying-systems-fact-sheet?fbclid=IwAR1iec2gGz_WlU-EprVIaC8jJnSPbR4qk3iPJO5MCfir3K1NqQys2zObB5c, 30 July 2022.

Jittanit, W., Saeteaw, N., Charoenchaisri, A. 2010. Industrial paddy drying and energy saving options. J. Stored. Prod. Res. 46: 209–213. doi.org/10.1016/j.jspr.2010.04.005

Jouppila, V.T., Gadsden, S.A., Bone, G.M., Ellman, A.U., Habibi, S.R. 2014. Sliding mode control of a pneumatic muscle actuator system with a PWM strategy. Int. J. Fluid Power 15: 19–31. doi.org/10.1080/14399776.2014.893707

Khanali, M., Giglou, A.K., Rafiee, S. 2018. Model development for shelled corn drying in a plug flow fluidized bed dryer. Eng. Agric. Environ. Food 11: 1–8. doi.org/10.1016/j.eaef.2017.09.002

McCormack, A.S., Godfrey, K.R. 1998. Rule-based autotuning based on frequency domain identification. IEEE T. Contr. Syst. T. 6: 43–61. doi: 10.1109/87.654876

Mondal, M.H.T., Shiplu, K.S.P., Sen, K.P., Roy, J., Sarker, M.S.H. 2019. Performance evaluation of small scale energy efficient mixed flow dryer for drying of high moisture paddy. Dry. Technol. 37: 1541–1550. doi.org/10.1080/07373937.2018.1518914

Müller, A., Nunes, M.T., Maldaner, V., et al. 2022. Rice drying, storage and processing: Effects of post-harvest operations on grain quality. Rice Sci. 29: 16–30. doi.org/10.1016/j.rsci.2021.12.002

Mustafa, Y., Pracha, B., Nifahmee, H. 2014. Must flow dryer for rough rice. In: Proceedings of 3rd International Conference on Green Computing, Technology and Innovation, the Asia Pacific University of Technology and Innovation. Malaysia, pp. 26–30.

Ogata, K. 2010. Modern Control Engineering, Vol. 5. Prentice Hall. Upper Saddle River, NJ, USA,

Pakdeekaew, A. 2021. Development of methods for real time measuring and evaluating the paddy moisture content. M.Eng. thesis, School of Mechanical Engineering, Suranaree University of Technology. Nakhon Ratchasima, Thailand. [in Thai]

Sila, B., Pakdeekaew, A., Treeamnuk, K., Treeamnuk, T. 2022. Effect of exhaust air recirculation on energy consumption in air heating system. In: Proceedings of 14th Conference of Electrical Engineering Network 2022. Phuket, Thailand, pp. 68–74. [in Thai]

Tuaynak, P., Chuchonak, M., Yapa, M., Bunyawanichkul, P. 2014. Influences of flow velocity of hot air to moisture content reduction of paddy in must flow paddy dryer. SWU Engineer. J. 9: 28–35. [in Thai]

Vengsungnle, P., Jongpluempiti, J., Pannucharoenwong, N., Echaroj, S., Wichangarm, M., Benjapiyaporn, C., Suthapan, W. 2018. Energy saving from heat recovery in paddy drying process. In: Proceedings of 2018 IEEE 5th International Conference on Engineering Technologies and Applied Sciences. Bangkok, Thailand, pp. 1–5.